
Article:
Dubois, M., Achon, I., Brench, R.A. et al. (2023) SIAMESE-RELATED1 imposes differentiation of stomatal lineage ground cells into pavement cells. Nature Plants, 9 (7). pp. 1143-1153. ISSN: 2055-026X

https://doi.org/10.1038/s41477-023-01452-7

SIAMESE-RELATED1 imposes differentiation of stomatal lineage ground cells into pavement cells

Marieke Dubois[1,2], Ignacio Achon[1,2], Robert A. Brench[3], Stefanie Polyn[1,2], Ruben Tenorio Berrio[1,2], Ilse Vercauteren[1,2], Julie E. Gray[3], Dirk Inzé[1,2] and Lieven De Veylder[1,2]*

[1]Department of Plant Biotechnology and Bioinformatics, Ghent University, 9052 Gent, Belgium.

[2]Center for Plant Systems Biology, VIB, 9052 Gent, Belgium.

[3]School of Biosciences, University of Sheffield, Sheffield S10 2TN, UK

*Corresponding author. Email: lieven.deveylder@psb.vib-ugent.be.

One-Sentence Summary: SMR1 controls pavement cell over stomata ratio through imposing differentiation of stomatal lineage ground cells into pavement cells.

The leaf epidermis represents a multifunctional tissue consisting of trichomes, pavement cells and stomata, the specialized cellular pores of the leaf. Pavement cells and stomata both originate from regulated divisions of stomatal lineage ground cells (SLGCs) but, strikingly, whereas the ontogeny of the stomata is well characterized, the genetic pathways activating pavement cell differentiation remain relatively unexplored. Here, we reveal that the cell cycle inhibitor SIAMESE-RELATED1 (SMR1) is essential for timely differentiation of SLGCs into pavement cells by terminating SLGC self-renewal potency, which depends on CYCLIN A proteins (CYCAs) and CYCLIN-DEPENDENT KINASE B1 (CDKB1). By controlling SLGC-to-pavement cell differentiation, SMR1 determines the ratio of pavement cells to stomata, and adjusts epidermal development to suit environmental conditions. We therefore propose SMR1 as an attractive target for engineering climate-resilient plants.

The leaf epidermis represents a multifunctional tissue that contributes to the water balance, gas exchanges and defense against pathogens, as well as the protection of the underlying mesophyll cells from physical damage[1-4]. To achieve these many functions, the leaf epidermis is composed of different cell types, each with characteristic shapes and sizes and of which the density specifies the leaf's physiology. Typically, the epidermis holds trichomes, stomata and pavement cells that all arise from undifferentiated protodermal cells.

Within dicots, the pavement cells appear as interlocking pieces of a jigsaw puzzle, with the lobes and sinuses of neighboring cells interdigitating perfectly, providing mechanical strength, while still being of sufficient flexibility to allow multidirectional growth of the leaf lamina[1]. Strikingly, whereas stomata and trichome ontogeny have been well-described, the molecular pathways that trigger early differentiation of pavement cells are largely unknown and it is currently not clear whether pavement cell specification requires a specific gene regulatory program[5]. About half of the pavement cells differentiate directly from protodermal precursors, whereas the other half arise as secondary products from stomatal lineage divisions[6]. The stomatal lineage starts with the conversion of a subset of protodermal cells into meristemoid mother cells (MMCs). These MMCs most frequently undergo an asymmetric cell division that generates a triangular-shaped meristemoid and a larger stomatal lineage ground cell (SLGC). The meristemoid can either differentiate directly into a pair of guard cells following a symmetric guard mother cell (GMC) division or undergo up to three rounds of amplifying asymmetric cell divisions, resulting in the formation of additional SLGCs. The SLGC retains a flexible potency to self-renew, either differentiating directly into a pavement cell or undergoing a spacing cell division that gives rise to an additional meristemoid[7,8].

Currently, the factors that grant the SLGCs self-renewal potency are largely unknown. Within Arabidopsis, two putative regulators are the potential transcriptional repressors DEK and

DEK-like that are expressed in the stomatal lineage but stronger in SLGCs[9]. Mutation of both genes results in a reduced stomatal density, which suggests that DEK and DEK-like promote SLGCs to undergo spacing cell divisions. Another candidate factor is the R2R3 MYB transcription factor MYB16. Expression of *MYB16* is enriched in SLGCs and expression of a dominant-negative allele results in a decreased stomatal density, suggesting that MYB16 might inhibit premature differentiation of SLGCs into pavement cells[9]. In contrast, putative factors that terminate the self-renewal potency of SLGCs have not been reported so far.

Transcriptional profiling of stomatal lineage cell types demonstrated that SLGCs show a transcriptomic signature between cell division and differentiation. For example, SLGC transcripts are enriched for both inhibitors and activators of the anaphase promoting complex/cyclosome (APC/C) E3-ubiquitin ligase that marks cell cycle proteins for destruction[9]. Among these, the *CELL CYCLE SWITCH 52 A1* and *A2* (*CCS52A1* and *CCS52A2*) genes control endocycle onset in leaves, being an alternative cell cycle during which DNA duplication is not followed by mitosis and cytokinesis, resulting in a stepwise increase in the cell's DNA content[10,11]. With polyploidy being a hallmark of differentiated cells, endocycle onset possibly marks the loss of the SLGCs self-renewal capacity.

Next to the APC/C, cell cycle exit and endocycle onset is controlled by the plant-specific cyclin-dependent kinase (CDK) inhibitory proteins SIAMESE (SIM) and SIAMESE-RELATED1 (SMR1). SIM controls the mitotic-to-endocycle transition in trichomes[12], whereas SMR1 (also known as LOSS OF GIANT CELLS FROM ORGANS (LGO)) has been implicated in the control of endoreplication in leaves and sepals[13]. Differently, the closely related family member SMR4 was reported to be expressed at the meristemoid-to-GMC transition, accounting for a cell cycle deceleration that marks the switch from the meristemoid's asymmetric cell division to the symmetric cell division that produces the two guard cells[14]. Accordingly, knockout of *SMR4*

results in an increased number of stomata and stomatal precursor cells, whereas its stomatal-lineage specific overexpression results in an extension of the G1 phase of the MMCs, generating irregularly shaped meristemoid and stomata composed of skewed guard cells. These data illustrate that an SMR4-dependent cell cycle extension is important for the proliferation-to-differentiation switch within the stomatal lineage. Differently, here we demonstrate that SMR1 terminates the self-renewal potency of the SLGCs, preventing them to re-enter the cell cycle. In such manner, SMR1 triggers SLGC-to-pavement cell differentiation, allowing leaves to adapt to drought through the control of stomatal density.

Results

SMR1 controls the timing of SLGC cell cycle exit

To visualize the role of SMR1 during leaf development, we benchmarked its expression pattern against that of the *CDKB1;1* mitotic cell cycle marker during the maturation of the first leaf, using *pCDKB1;1:GUS* and *pSMR1:GFP-GUS* reporter lines. Within the young proliferating leaf, the *pCDKB1;1:GUS* reporter was found to be uniformly expressed. As the leaf matured, the expression basipetally disappeared, becoming confined to the vascular cells, stomatal precursor cells and guard cells (Supplementary Fig. 1a), fitting with the described pattern of cell proliferation exit in leaves[15,16]. The *pSMR1:GFP-GUS* reporter line displayed the reciprocal expression pattern, appearing first at the tip of the young leaf and eventually spreading out over the complete leaf (Supplementary Fig. 1b), corresponding to its role as cell cycle inhibitor.

To map the cellular role of SMR1 during leaf development, we performed a kinematic leaf growth analysis of wild-type versus *smr1* mutant plants. Whereas both genotypes displayed an equal leaf area (Fig. 1a), *smr1* leaves accumulated over time more epidermal cells compared to the wild type (Fig. 1b). This cell number increase was solely attributed to the pavement cells (Fig. 1c),

which were smaller than those of the wild type (Fig. 1d). Instead, the number of stomatal cells tended to be lower in *smr1*, particularly during the first days of leaf development (Fig. 1e). This translated into a significant drop in the stomatal index (being the number of stomata divided by the total number of epidermal cells) (Fig. 1f). These data suggest that SMR1 specifically controls pavement cell number.

To understand the specific effect of SMR1 on pavement cells, we visualized *SMR1* expression in the epidermis. Within the stomatal lineage, *pSMR1:GFP-GUS* was absent in the meristemoids and SLGCs (Fig. 1g), including those undergoing a spacing cell division (Fig. 1h). Correlated with the appearance of lobes and sinuses, the cells gained a GFP signal (Fig. 1i) and eventually all cells surrounding the stoma became GFP-positive (Fig. 1j). These data suggest that SMR1 might control the timing of the cell cycle exit of the SLGCs. To test this hypothesis, we introgressed the *pCDKB1;1:GUS* marker in the *smr1* mutant background. Except for the stomata, epidermal cells did not show *pCDKB1;1:GUS* expression within a 10-day-old first leaf of the wild type (Fig. 2a). In contrast, expression was maintained in the SLGCs and pavement cells in the *smr1* mutant (Fig. 2a; Supplementary Fig. 1c), indicating that in the absence of SMR1, these cells remained mitotically active for a longer time.

SMR1 is required for SLGC-to-pavement-cell differentiation

Hypothesizing that SMR1 arrests cell cycle progression in SLGCs, thereby stimulating their differentiation to pavement cells, we tracked the behavior of epidermal cells over a period of five days, from 10 to 14 days after stratification (DAS). In accordance with the *pCDKB1;1:GUS* expression pattern (Supplementary Fig. 1), very few pavement cells underwent cell division in wild-type leaves during this time period (Fig. 2b). In contrast, in the *smr1* mutant, two different types of pavement cell divisions were observed (Fig. 2b). Among the seemingly differentiated

pavement cells, around 20% underwent a symmetric cell division within the 5-day period (Fig. 2b, blue cells), indicating that SMR1 plays a role in restraining differentiated pavement cells to divide. Strikingly, about one out of ten seemingly differentiated pavement cells underwent a series of asymmetric cell divisions resembling those of the stomatal pathway, to eventually yield a new stomatal complex, including the generation of extra stomata and pavement cells (Fig. 2b, light-green cells). This type of stomatal-lineage-like divisions was never observed in wild-type leaves of the same age and suggested that the puzzle-shaped cells in the *smr1* background maintained the self-renewal capacity, as if they still had the SLGC identity. Accordingly, compared to the wild type, *smr1* leaves displayed a prolonged expression of genes that were previously associated with the division potential of SLGCs[9] (Fig. 2c). These data could suggest that part of the *smr1* pavement cells maintained a SLGC-like behavior. Supporting this, *TOO MANY MOUTHS* (*TMM*) and *SPEECHLESS* (*SPCH*), which are exclusively expressed in stomatal lineage cells[17-19], could be detected within about ~3% and ~6% of the pavement cells in *smr1*, respectively (Fig. 2d-h).

SPCH plays a direct role in regulating asymmetric cell division in the stomatal lineage[17]. Accordingly, when SPCH activity was abolished in the *smr1 spch-3* double mutant, the epidermis showed pavement cells that still divided symmetrically, while asymmetric divisions could not be detected (Supplementary Fig. 2). Interestingly, whereas cotyledons of the *spch-3* mutant lost expression of *TMM*, which is in accordance with a previous report[20], abolishing SMR1 activity in the *smr1 spch-3* double mutant strongly increased *TMM* expression to levels exceeding that of wild-type leaves (Supplementary Fig. 2c). Because no stomatal lineage cells are observed in these mutants, the *TMM* expression likely originates from the puzzle-shaped epidermal cells. Altogether, these results demonstrate that a fraction of the puzzle-piece shaped epidermal cells in the *smr1* mutants do not maintain a fully differentiated pavement cell behavior, despite their appearance.

Instead, they behave like SLGCs, undergoing multiple divisions and eventually giving rise to new stomata.

SMR1 acts through CYCLIN A2–CDKB1 complexes

The plant-specific CDKB1;1 protein associates with SMR1[21] and controls stomatal lineage divisions together with CDKB1;2[22,23], suggesting that B1-type CDKs might be targeted by SMR1 for the differentiation of SLGCs into pavement cells. Knockout of both B1-type CDKs in the *smr1* background resulted in a strong suppression of both the symmetric and asymmetric pavement cell division rates (Fig. 3). A2-type cyclins participate with CDKB1s in the formation of stomata[24]. Accordingly, when comparing an *smr1 cyca2;1 cyca2;3 cyc3;4* quadruple mutant with *smr1*, again a reduction of both pavement cell division types was observed (Fig. 3). These data suggest that SMR1 predominantly controls the exit from the pavement cell division program through inhibition of CYCA2-CDKB1 complexes, although some residual cell division activity suggests the involvement of other cyclin-CDK complexes as well.

SMR1 activity is sufficient to impose pavement cell differentiation

To test whether SMR1 activity is sufficient to drive pavement cell differentiation, we ectopically expressed a *SMR1-GFP* fusion protein that complemented the *smr1* mutant[25] in the leaf either using the constitutively active *CaMV35S* promoter (named *SMR1^{OE}*), or the stomatal lineage-specific *TMM* promoter[26]. Constitutive expression caused a strong reduction in the number of both pavement cells and stomata, resulting in a reduced leaf area (Supplementary Fig. 3). Strikingly, we observed aberrant stomata in which the final division, to generate the pair of guard cells, did not take place (Supplementary Fig. 3), resembling the phenotype of plants with a reduced CDKB1-CYCA2 activity[22,24].

In contrast, *pTMM:SMR1-GFP* seedlings did not develop beyond the cotyledon stage, with 5-day-old cotyledons being strongly reduced in size, compared to control plants (Fig. 4a). When analyzing the *pTMM:SMR1-GFP* cotyledons at cellular level, no stomata could be detected within the abaxial epidermis that consisted only of cells with a pavement cell morphology (Fig. 4b). Among these, we observed cells bearing an SMR1-GFP signal, thus deriving from stomatal precursor cells, illustrating that SMR1 activity imposes pavement cell differentiation on stomatal lineage cells. Correspondingly, the expression level of genes that were previously associated with SLGC self-renewal was reduced in the *pTMM:SMR1-GFP* cotyledons (Fig. 4c).

Reduced ploidy levels do not cause a stomatal index change

SMR1 has previously been associated with increasing cellular ploidy levels in leaves and sepals[27]. In the Arabidopsis leaf, at least two major pathways control endoreplication onset: either through destruction of cyclins by the activity of the APC/C subunits CCS52A1 and CCS52A2, or through G2/M-specific CDK inhibition by SMR1[28]. To study whether endoreplication is a general trigger of early pavement cell differentiation, thereby controlling the ratio between stomata and pavement cells, we analyzed the epidermis in plants knocked-out for *CCS52A1* and ectopically expressing the transcriptional repressor DEL1 (*DEL1*^{OE}), as a proxy for *CCS52A2* knockdown[11]. Using dual-color flow cytometry, we first compared the ploidy levels in leaf epidermal cells of wild-type versus *smr1* and *ccs52a1 DEL1*^{OE} plants. This strategy is based on epidermis-specific expression of a nuclear-targeted histone-GFP fusion (Supplementary Fig. 4), enabling ploidy measurements in the epidermal cells only. Compared to the wild type, *ccs52a1 DEL1*^{OE} double mutant leaves displayed a clearly decreased number of 8C and 16C-ploidy epidermal cells (Fig. 5a) to a level similar to that of the *smr1* mutant. Accordingly, the pavement cell area of the *ccs52a1 DEL1*^{OE} double mutant was reduced compared to the wild type, similarly to what was observed for the *smr1*

mutant (Fig. 5b). Strikingly, whereas both lines displayed an equal increase in epidermal cell number (Fig. 5c), in the *ccs52a1 DEL1*^{OE} double mutant both an increase in pavement and stomatal cell number was observed (Fig. 5d,e). This resulted in a stomatal index being identical to that of control plants (Fig. 5f), whereas the stomatal index dropped in the *smr1* mutant. Altogether, these results suggested that reduced ploidy levels *in se* cannot explain the epidermal phenotypes observed in the *smr1* mutant.

SMR1 determines stomatal density under drought conditions

Stomatal lineage divisions operate downstream of environmental cues, including carbon dioxide availability, high temperature and water shortage[29]. As *SMR1* transcripts are induced under water deficiency[25], we exposed the *smr1* mutant and the *SMR1*^{OE} plants to severe drought by withholding watering of 5-week-old plants. The *smr1* plants did not show any measurable difference compared to the wild type in terms of stomatal conductance (Fig. 6a), leaf temperature (Fig. 6b), or soil moisture (Fig. 6c). Yet, *smr1* plants showed the tendency to wilt slightly more than the wild type (Fig. 6d), a weak effect that was observed in independent experiments when measuring the rosette area reduction caused by drought and the relative water content (Supplementary Fig. 5). On the contrary, the *SMR1*^{OE} plants showed a reduced stomatal conductivity (Fig. 6a), displayed a slightly higher leaf temperature (Fig. 6b) and maintained a significantly higher soil moisture for a longer time (Fig. 6c). Correspondingly, although *SMR1*^{OE} rosettes were more compact than those of wild-type plants under well-watered conditions, *SMR1*^{OE} clearly displayed less wilting compared to control plants after drought (Fig. 6d).

To understand the cellular basis of the observed differences in drought sensitivity of *SMR1*^{OE} and *smr1* plants, we analyzed the effect of drought on the epidermis. For this purpose, we used the Weighing, Imaging and Watering Machine (WIWAM) platform[30], applying mild drought

earlier during leaf development (9 DAS). This type of drought does not trigger wilting, but allows the leaves to adapt their cellular composition to the stress. After 10 days of moderate drought, the leaf area of wild-type plants, *smr1* mutants and *SMR1*^{OE} plants was reduced to a similar extent (-25%, -28% and -20%, respectively; Fig. 6e), but the genotypes exhibited a distinct cellular response. Pavement cell size was significantly affected by mild drought in the *SMR1*^{OE} plants only (Fig. 6f), whereas the wild type and *smr1* mutant showed a reduction in total epidermal cell number (Fig. 6g). Wild-type and *smr1* leaves showed both ~20% less pavement cells under drought, while no pavement cell number reduction was observed in *SMR1*^{OE} leaves, possibly because these plants have less pavement cells even under well-watered conditions (Fig. 6h). Similarly, the number of stomata in the *SMR1*^{OE} leaves was low under well-watered conditions and remains equally low under drought (Fig. 6i). Strikingly, while wild-type plants reduced the number of stomata under drought (Fig. 6i), thereby adjusting their stomatal density to the stress conditions as reported previously[31], *smr1* mutants failed to do so (Fig. 6j). Altogether, these results suggest that SMR1 contributes to drought stress adaptation by controlling the stomatal density, and that higher expression of *SMR1* (as in *SMR1*^{OE}) allows plants to reduce the number of stomata, thereby avoiding drought stress response better than wild-type plants.

Discussion

Does SMR1 act as cell fate regulator?

Previously, SMR1 has been described as a stochastic activator of endocycle onset, being accountable for the variation in size observed among sepal epidermal cells[13]. Here, we demonstrate that SMR1 additionally terminates the self-renewal capacity of the SLGCs and triggers pavement cell differentiation, as such controlling the leaf total pavement cell number. This work raises the

question of what exactly determines the transition of an SLGC to a pavement cell. Within *smr1* leaves, seemingly differentiated pavement cells were observed to undergo symmetric and asymmetric cell divisions, the latter mimicking stomatal lineage division patterns, resulting in the formation of new stomatal complexes. The data suggest that a lobed epidermal cell can still behave like an SLGC, as observed in *smr1*, excluding that the lobed cell shape is the sole determinant of pavement cell identity. Supporting this, expression analysis by by real-time quantitative PCR (RT-qPCR) showed that the pavement cells of the *smr1 spch-3* double mutant strongly express *TMM*, despite their lobed appearance. Alternatively, a role for endoreplication in the pavement cell differentiation process might be suggested, considering the enrichment of components of the APC/C controlling endocycle onset[9] in SLGCs and the reported inhibition of full trichome cell differentiation upon inhibition of endocycle onset in trichome precursor cells[32]. Likewise, the observed trichoblast- and atrichoblast-specific expression pattern for respectively *SIM* and *SMR1* in root transition zone cells suggests a role for these CDK inhibitors in the differentiation of these tissue types[33]. However, differently from the *smr1* mutant, in which the SLGC-like behavior of the epidermal cells caused an imbalanced ratio of stomata over pavement cells, the *ccs52a1 DEL1*^{OE} mutant maintained a stomatal index equal to the wild type. Combined with previously published leaf ploidy maps showing that differentiated pavement cells can have a 2C nuclear content[34], these results suggest that endoreplication is not a main trigger of pavement cell identity. Finally, as can be observed in Figure 2b, some of the wild-type pavement cells that are smaller than *smr1* mutant epidermal cells do not undergo divisions, supporting the hypothesis that cell size *in se* does not determine pavement cell fate. Altogether, this suggests that SMR1 might impose pavement cell differentiation by acting directly on cell fate determinants, of which the precise nature is yet unknown.

Molecular convergence to SPCH downstream of SMR1

Our genetic data indicate that SMR1 operates at least in part through targeting the CDKB1/CYCA2 complex. Nevertheless, other CDK complexes probably also need to be repressed, as in the corresponding higher-order mutants still some residual symmetric and asymmetric cell divisions could be observed. Correspondingly, both biochemical and genetic data have illustrated that the closely related SIM inhibitor targets both A- and B1-type CDKs[35,36]. SPCH is positively controlled by CDKA;1 phosphorylation, likely controlling its stability[37]. Expression of the phosphorylation-mimic *SPCH*^{186D} mutant restores the defects in the stomatal development of a dominant-negative *CDKA;1* allele, whereas expression of a phosphorylation-deficient version fails to rescue the *spch* lack of stomata phenotype. Combined, these data let us speculate that following the transcriptional activation of *SMR1*, SLGCs might initiate differentiation towards pavement cells through SPCH degradation via the inhibition of CDK activity. Correspondingly, we could detect SPCH-GFP accumulation in *smr1* pavement cells. Analogously, ectopic expression of *SMR1* in MMCs might impose pavement cell differentiation through loss of SPCH activity. Differently, the symmetrical pavement cell divisions appear to be SPCH independent, as they were still observed in the *smr1 spch-3* double mutant.

Towards engineering climate-resilience by modulating *SMR1* expression

Combined with the recently reported role for SMR4 in controlling the meristemoid-to-guard mother cell transition switch by inducing a deceleration from the cell cycle[14], our data about SMR1 controlling stomatal density by terminating SLGC self-renewal activity suggest that SMR proteins represent an important class of developmentally controlled cell cycle inhibitory proteins. Next to its described role in triggering endoreplication, SMR1 steers division and growth of pavement

cells, modulating the stomatal density, in this way directly controlling both leaf growth and physiology. By inducing *SMR1* expression in changing environments, such as upon water deficiency, plants adjust the cellular composition of the evaporative leaf tissue, reducing the numbers of stomata per area. In the absence of SMR1, plants fail to maintain a low stomatal density under drought conditions, which results in plants with slightly more pronounced wilting. In contrast, overexpressing *SMR1* allows plants to be more resilient to severe drought, with reduced wilting and water use. By reducing the number of stomata and pavement cell divisions even under well-watered conditions, *SMR1*-overexpressing plants limit the evaporative leaf surface, resulting in stunted growth but improved resilience. These results are in line with previous observations that smaller plants tend to resist better to severe drought, because of less evaporation and a different distribution of energy-resources towards survival to severe stress, rather than organ growth[38]. However, because plant yield under drought, rather than resilience, is currently seen as a major goal in applied and academic research of drought tolerance, engineering *SMR1* expression still requires fine-tuning. Given the negative effect of *SMR1*-overexpression on plant growth under control conditions, we speculate that *SMR1* levels should remain low as long as water is abundant. Upregulating *SMR1* expression in a drought-inducible manner, specifically in the leaf epidermis, might be a promising approach to reduce the stomatal density under drought, yielding plants with an increased drought-tolerance without growth penalty. Alternatively, identifying the downstream targets of SMR1 (under drought) might allow to uncouple the role of SMR1 in symmetric versus asymmetric division of pavement cells. We speculate that such insights would enable the engineering of reduced stomatal density under drought, while allowing the pavement cell division to proceed, thereby allowing leaf growth under drought with reduced water evaporation through the pores.

Methods

Plant lines and growth conditions

The mutant lines *smr1* (SALK_0339050), *SMR1*^{OE}, *spch-3* (SAIL_36_B06), *ccs52a1* (SALK_083656), *DEL1*^{oe}, *cdkb1;1* (SALK_073457) *cdkb1;2* (SALK_ 133560), *cyca2;1* (SALK_121077), *cyca2;3* (SALK_092515) and *cyca2;4* (SALK_070301) have been described previously[11,17,24,25,39,40]. Genotyping primers are given in Supplementary Table 1. Double and triple mutants were made by crossing these lines. The transcriptional reporter line *pCDKB1;1:GUS* was described by Boudolf et al.[22]. To construct the *pCER6:H2A-eGFP* vector (Supplementary Fig. 4A), the *ECERIFERUM 6* (*CER6, AT1G68530*) sequence was amplified from genomic DNA by PCR. The PCR product was purified and cloned into the *pDONRP4P1r* vector (Thermo Fisher Scientific). The promoter fragment was then assembled with GAL4 into the *pB-9FH2A-UAS-7m24GW* destination vector in a multi-site Gateway reaction to create an activator construct using the LR Clonase II+ (Thermo Fisher Scientific). This destination vector contains a *HISTONE 2A-6* (*H2A*)-encoding sequence fused to *eGFP* and driven by the repetitive UAS promoter, as described[41]. To construct the *pSMR1*:*GFP-GUS* transcriptional reporter, the *SMR1* (AT3G10525) promoter, 2100 bp upstream of the ATG codon, was amplified from genomic DNA by PCR. The PCR product was purified and cloned into pDONR221 vector (Thermo Fisher Scientific) and subsequently recombined into pMK7S*NFm14GW[42] using the LR Clonase II+ (Thermo Fisher Scientific). To generate the *pTMM*:*SMR1-GFP* construct, the pGG-A-pTMM-B vector[43], along with the pGG-C-SMR1-D vector, were used in a Golden Gate reaction having pFASTRK-A-G as the destination vector.

All constructs were transformed via heat-shock into ccdB-sensitive DH5α *Escherichia coli*. Depending on the selectable marker, the cells were plated on LB medium containing 100 mg/mL carbenicillin, 100 μg/mL spectinomycin, 25 μg/mL kanamycin, or 10 μg/mL gentamycin.

Colonies were verified via colony PCR, restriction digestion and/or Sanger sequencing by Eurofins Scientific. All constructs were transferred into the *Agrobacterium tumefaciens* C58CRifR strain harboring the pMP90 plasmid. The obtained Agrobacterium strains were used to generate stably transformed Arabidopsis (Col-0) using the floral dip transformation method[44]. Successful transformants were selected using kanamycin or a fluorescence microscope in the case of FAST constructs. For imaging of *pTMM:SMR1-GFP*, T0 (primary transformants) were used, given that plants are lethal after the cotyledon stage. Seeds were sterilized with 100% ethanol followed by 40% bleach, after which they were washed several times. For all experiments, seeds were stratified in the dark for 2 days at 4ºC. Unless stated otherwise, plants were grown *in vitro* under long-day conditions (16 h light/8 h dark, Lumilux Cool White lm, 50 to 70 µmol m-2s-1) at 21ºC on agar-solidified culture medium (Murashige and Skoog [MS] medium, 10 g/L saccharose, 2.15 g/L MS, 0.5 g/L 2-(N-morpholino) ethanesulfonic acid [MES], and 0.8% plant tissue culture agar). For analysis of leaf parameters, including confocal imaging, plants were grown in horizontal petri dishes.

Drought treatment

For the moderate drought treatments, seeds were sown in pots, which were filled up to 85 g ± 0.5 g of Saniflor soil (Van Israel N.V., Geraardsbergen, Belgium) with an absolute water content of on average 70%. After 3 nights of stratification at 4ºC in darkness, the pots were moved to the automated phenotyping platform WIWAM (21ºC and 16 h light/8 h dark) and randomized to homogeneously mix the three genotypes. The plants were watered daily to obtain a relative humidity of 2.2 g_{water}/g_{soil}. The drought stress was initiated at 9 DAS and the relative humidity dropped to on average 1.2 g_{water}/g_{soil}. For the moderate drought treatment, the soil humidity was kept at this level until the end of the experiment, at 19 DAS.

For long drought treatment, seeds were sown on M3 compost:perlite (4:1) and stratified on soil (72h at 4°C in darkness) and subsequently transferred to a growth chamber (Conviron model BDR16) at 21°C:16°C day/night. Light was 150 µmol m^{-2} s^{-1} for 12 h. After 5 weeks, plants were moved to a controlled temperature room for thermal imaging and water was withheld for drought treatment. Soil moisture readings were taken from five pots per genotype per repeat at three locations per pot using a calibrated moisture probe from Delta T Devices (accuracy ± 1%). Pots (and plants) were weighed each day to monitor water loss.

Stomatal conductance and assimilation assay

For stomatal conductance measurements, a LI-6800 portable photosynthesis system (LiCor, Lincoln, NE, USA) was used as infrared gas analyzer (IRGA) on 7-week-old plants. Mature leaves were measured 4-7 h after the start of the photoperiod. Chamber relative humidity was kept at 60%, flow rate at 400 µmol s^{-1} and temperature was set to 21°C. Light intensity was maintained at 500 µmol m^{-2} s^{-1} and carbon dioxide at 400 ppm. Leaves were allowed to equilibrate in the chamber for 20-30 min before measurements started. Reading were logged every 30 s for 15 min. Five plants per genotype were analyzed.

Thermal imaging

A FLIR SC 660 thermal imaging camera (FLIR Systems, Wilsonville, OR, USA) was used to take infrared images of 5-week-old plants for 15 days after the onset of drought. Images were taken 2 h after the start of the photoperiod. The data of the first 30-min period after leaving the growth room was discarded to allow the plants and room to equilibrate. Images from the following 90 min were used. Temperatures from the center of three mature leaves per plant were measured and an average leaf temperature per plant was calculated. Five plants per genotype per repeat were measured.

Flow cytometry

For ploidy analysis, leaf material was chopped on a Petri dish with a razor blade in 1 mL of ice cold Galbraith's nuclei extraction buffer (45 mM $MgCl_2$, 20 mM MOPS, 30 mM sodium citrate, 0.1% [v/v] Triton X-100, adjusted to pH 7.0 using 1 M NaOH). The homogenate was passed through a 50-µm Cell Trics filter. Thereafter, 2.5 µL DAPI (1 mg/mL concentration) was added to stain the DNA. The DNA content was measured using a Quantum P (Quantum Analysis) flow cytometer excited by illumination at 395 nm and equipped with an additional 488-nm laser to excite and detect GFP-specific fluorescence. The ploidy levels (2C, 4C, 8C and 16C fractions) of GFP-positive cells and total leaf cells were determined from DAPI fluorescence measurements using the "Ploidy Analysis" tool of CyPad software (Quantum Analysis). To calculate the endoreplication index, the following formula was used, with %*n*C representing the fraction of nuclei with *n* times the haploid genome content: 0 X %2C + 1 X %4C + 2 X %8C + 3 X %16C + 4 X %32C.

Kinematic leaf growth analysis

Kinematic analysis of the abaxial epidermal cells of leaves was performed as described[45]. Briefly, seeds were germinated in round 12-cm Petri dishes. From 8 until 21 DAS, first leaves were harvested. Leaf samples were cleared overnight in ethanol, and subsequently stored in lactic acid for microscopy. The total leaf area (blade) was determined directly with a charge-coupled device camera mounted on a Stemi SV11 microscope (Zeiss), and ImageJ (https://imagej.nih.gov/ij/) was used for measurement. A Leica DMLB microscope with a drawing-tube attached was used to generate drawings of outlines of at least 50 cells of the abaxial epidermis located 25% and 75% from the distance between the tip and the base of the leaf lamina, halfway between the midrib and

the leaf margin. Scanned drawing-tube images of these groups of cells were used to measure the total drawn area (using the wand tool of ImageJ). Afterwards, the number of pavement cells and stomata in that area were determined, and the number of epidermal cells per leaf, epidermal cell size and stomatal index (number of stomata divided by total number of epidermal cells, including guard cells) were calculated. Cellular drawings were analyzed with a script[16] allowing the automatic measurement of each individual pavement cell area.

Leaf imprints

To track the pavement cell division within the first pair of leaves from 10 to 14 DAS, seeds were sown in soil. After 3 DAS at 4ºC in darkness, the pots were moved to a growth chamber (21ºC and 16 h light/8 h dark). An imprint of the abaxial surface of the leaf was taken with dental resin (polyvinyl impression material, Genie Light Body Fast set Std). For the subsequent cellular analysis, the leaf imprints were overlaid with a thin layer of nail polish. The nail polish copy of the imprint was analyzed by scanning electron microscopy (TM-1000, Hitachi). Four to seven leaves were analyzed per line. For each region, approximately 120 cells were followed over a 5-day period, and the number of pavement divisions (symmetrical and stomatal) within that region throughout this time-lapse was counted. Cell division rates were calculated by dividing the number of observed divisions by the starting cell number and number of days.

Histochemical GUS assay

Leaves and/or whole seedlings were fixed in an ice-cold 80% [v/v] acetone solution for 30 min. Samples were washed several times with phosphate buffer (14 mM NaH_2PO_4 and 36 mM Na_2HPO_4) prior to incubation in staining buffer (0.5 mg/mL 5-bromo-4-chloro-3-indolyl-β-D-

glucuronic acid, 0.165 mg/mL potassium ferricyanide, 0.211 mg/mL potassiumferrocyanide, 0.585 mg/mL EDTA pH 8, and 0.1% [v/v] Triton-X100, dissolved in phosphate buffer) at 37°C between 2 and 12 h, until sufficient staining was observed.

Confocal microscopy

For visualization of epidermal leaf cells, leaves were incubated in a 10-μM PI solution to stain cell walls and imaged using an LSM 5 Exciter (Zeiss) confocal microscope. For PI and GFP excitation, the 544 line of a HeNe laser and the 488 line of an Argon laser were used, respectively. Laser light passed through an HFT 405/488/543/633 primary dichroic beam splitter before reaching the sample, and emitted light from the sample first passed through an NFT 545 secondary dichroic beam splitter, after which it passed through a 650-nm long-pass filter for PI detection and through a 505- to 530-nm bandpass filter for detection of GFP. PI and GFP were detected simultaneously with the line scanning mode of the microscope.

RT-qPCR

RNA was isolated with the ReliaPrep RNA tissue miniprep system (Promega) and used for cDNA synthesis with the iScript cDNA synthesis kit (Bio-Rad). RT-qPCR was performed using the SYBR green kit (Roche) with 100 nM primers and 0.125 mL of RT reaction product in a total volume of 5 mL per reaction. Reactions were run and analyzed on the LightCycler 480 (Roche) according to the manufacturer's instructions with the use of the following reference genes for normalization: *EMB2386*, *PAC1* and *RPS26E*. For each reaction, three technical repeats and two to three biological repeats (see Figure legends) were performed. All primers sequences used for RT-qPCR are listed in Supplementary Table 1.

Statistical analysis

All statistical analyses were performed using GraphPad Prism v.9 (www.graphpad.com/features), except the data shown in Supplementary Fig. 5a, for which RStudio v.1.3.1073 (www.r-studio.com) was AQ12used. The tests that were used and the sample sizes are indicated in each figure legend, and all P values can be found in Supplementary Table 2.

Data availability

All data are available in the main text or the supplementary materials.

References

1 Liu, S., Jobert, F., Rahneshan, Z., Doyle, S. M. & Robert, S. Solving the puzzle of shape regulation in plant epidermal pavement cells. *Annu. Rev. Plant Biol.* **72**, 525-550 (2021). https://doi.org:10.1146/annurev-arplant-080720-081920

2 Glover, B. J. Differentiation in plant epidermal cells. *J. Exp. Bot.* **51**, 497-505 (2000). https://doi.org:10.1093/jexbot/51.344.497

3 Jacques, E., Verbelen, J.-P. & Vissenberg, K. Review on shape formation in epidermal pavement cells of the *Arabidopsis* leaf. *Funct. Plant Biol.* **41**, 914-921 (2014). https://doi.org:10.1071/FP13338

4 Javelle, M., Vernoud, V., Rogowsky, P. M. & Ingram, G. C. Epidermis: the formation and functions of a fundamental plant tissue. *New Phytol.* **189**, 17-39 (2011). https://doi.org:10.1111/j.1469-8137.2010.03514.x

5 Zuch, D. T. *et al.* Cell biology of the leaf epidermis: fate specification, morphogenesis and coordination. *Plant Cell* **34**, 209–227 (2022). https://doi.org:10.1093/plcell/koab250

6 Geisler, M., Nadeau, J. & Sack, F. D. Oriented asymmetric divisions that generate the stomatal spacing pattern in arabidopsis are disrupted by the *too many mouths* mutation. *Plant Cell* **12**, 2075-2086 (2000). https://doi.org:10.1105/tpc.12.11.2075

7 Pillitteri, L. J. & Dong, J. Stomatal development in Arabidopsis. *Arabidopsis Book* **11**, e0162 (2013). https://doi.org:10.1199/tab.0162

8 Shpak, E. D., McAbee, J. M., Pillitteri, L. J. & Torii, K. U. Stomatal patterning and differentiation by synergistic interactions of receptor kinases. *Science* **309**, 290-293 (2005). https://doi.org:10.1126/science.1109710

9 Ho, C.-M. K., Bringmann, M., Oshima, Y., Mitsuda, N. & Bergmann, D. C. Transcriptional profiling reveals signatures of latent developmental potential in *Arabidopsis* stomatal lineage ground cells. *Proc. Natl. Acad. Sci. USA* **118**, e2021682118 (2021). https://doi.org:10.1073/pnas.2021682118

10 De Veylder, L., Larkin, J. C. & Schnittger, A. Molecular control and function of endoreplication in development and physiology. *Trends Plant Sci.* **16**, 624-634 (2011). https://doi.org:10.1016/j.tplants.2011.07.001

11 Lammens, T. *et al.* Atypical E2F activity restrains APC/$C^{CCS52A2}$ function obligatory for endocycle onset. *Proc. Natl. Acad. Sci. USA* **105**, 14721-14726 (2008). https://doi.org:10.1073/pnas.0806510105

12 Churchman, M. L. *et al.* SIAMESE, a plant-specific cell cycle regulator, controls endoreplication onset in *Arabidopsis thaliana*. *Plant Cell* **18**, 3145-3157 (2006). https://doi.org:10.1105/tpc.106.044834

13 Roeder, A. H. *et al.* Variability in the control of cell division underlies sepal epidermal patterning in *Arabidopsis thaliana*. *PLoS Biol.* **8**, e1000367 (2010). https://doi.org:10.1371/journal.pbio.1000367

14 Han, S.-K. *et al.* Deceleration of the cell cycle underpins a switch from proliferative to terminal divisions in plant stomatal lineage. *Dev. Cell* **57**, 569-582 (2022). https://doi.org:10.1016/j.devcel.2022.01.014

15 Donnelly, P. M., Bonetta, D., Tsukaya, H., Dengler, R. E. & Dengler, N. G. Cell cycling and cell enlargement in developing leaves of *Arabidopsis*. *Dev. Biol.* **215**, 407-419 (1999). https://doi.org:10.1006/dbio.1999.9443

16 Andriankaja, M. *et al.* Exit from proliferation during leaf development in *Arabidopsis thaliana*: a not-so-gradual process. *Dev Cell* **22**, 64-78 (2012). https://doi.org:10.1016/j.devcel.2011.11.011
17 MacAlister, C. A., Ohashi-Ito, K. & Bergmann, D. C. Transcription factor control of asymmetric cell divisions that establish the stomatal lineage. *Nature* **445**, 537-540 (2007). https://doi.org:10.1038/nature05491
18 Lampard, G. R., Macalister, C. A. & Bergmann, D. C. Arabidopsis stomatal initiation is controlled by MAPK-mediated regulation of the bHLH SPEECHLESS. *Science* **322**, 1113-1116 (2008). https://doi.org:10.1126/science.1162263
19 Nadeau, J. A. & Sack, F. D. Control of stomatal distribution on the *Arabidopsis* leaf surface. *Science* **296**, 1697-1700 (2002). https://doi.org:10.1126/science.1069596
20 Horst, R. J. *et al.* Molecular framework of a regulatory circuit initiating two-dimensional spatial patterning of stomatal lineage. *PLoS Genet.* **11**, e1005374 (2015). https://doi.org:10.1371/journal.pgen.1005374
21 Van Leene, J. *et al.* Targeted interactomics reveals a complex core cell cycle machinery in *Arabidopsis thaliana*. *Mol. Syst. Biol.* **6**, 397 (2010). https://doi.org:10.1038/msb.2010.53
22 Boudolf, V. *et al.* B1-type cyclin-dependent kinases are essential for the formation of stomatal complexes in *Arabidopsis thaliana*. *Plant Cell* **16**, 945-955 (2004). https://doi.org:10.1105/tpc.021774
23 Xie, Z. *et al.* Regulation of cell proliferation in the stomatal lineage by the *Arabidopsis* MYB FOUR LIPS via direct targeting of core cell cycle genes. *Plant Cell* **22**, 2306-2321 (2010). https://doi.org:10.1105/tpc.110.074609
24 Vanneste, S. *et al.* Developmental regulation of CYCA2s contributes to tissue-specific proliferation in *Arabidopsis*. *EMBO J.* **30**, 3430-3441 (2011). https://doi.org:10.1038/emboj.2011.240
25 Dubois, M. *et al.* SIAMESE-RELATED1 Is Regulated Posttranslationally and Participates in Repression of Leaf Growth under Moderate Drought. *Plant Physiol.* **176**, 2834-2850 (2018). https://doi.org:10.1104/pp.17.01712
26 Bhave, N. S. *et al.* TOO MANY MOUTHS promotes cell fate progression in stomatal development of *Arabidopsis* stems. *Planta* **229**, 357-367 (2009). https://doi.org:10.1007/s00425-008-0835-9
27 Kumar, R. *et al.* Development of an efficient and reproducible regeneration system in wheat (*Triticum aestivum* L.). *Physiol. Mol. Biol. Plants* **23**, 945-954 (2017). https://doi.org:10.1007/s12298-017-0463-6
28 Bhosale, R., Maere, S. & De Veylder, L. Endoreplication as a potential driver of cell wall modifications. *Curr. Opin. Plant Biol.* **51**, 58-65 (2019). https://doi.org:10.1016/j.pbi.2019.04.003
29 Han, S.-K., Kwak, J. M. & Qi, X. Stomatal lineage control by developmental program and environmental cues. *Front. Plant Sci.* **12**, 751852 (2021). https://doi.org:10.3389/fpls.2021.751852
30 Skirycz, A. *et al.* Survival and growth of *Arabidopsis* plants given limited water are not equal. *Nat. Biotechnol.* **29**, 212-214 (2011). https://doi.org:10.1038/nbt.1800
31 Doheny-Adams, T., Hunt, L., Franks, P. J., Beerling, D. J. & Gray, J. E. Genetic manipulation of stomatal density influences stomatal size, plant growth and tolerance to restricted water supply across a growth carbon dioxide gradient. *Philos. Trans. R. Soc. Lond. B Biol. Sci.* **367**, 547-555 (2012). https://doi.org:10.1098/rstb.2011.0272
32 Bramsiepe, J. *et al.* Endoreplication controls cell fate maintenance. *PLoS Genet.* **6**, e1000996 (2010). https://doi.org:10.1371/journal.pgen.1000996
33 Bhosale, R. *et al.* A spatiotemporal DNA endoploidy map of the Arabidopsis root reveals roles for the endocycle in root development and stress adaptation. *Plant Cell* **30**, 2330-2351 (2018). https://doi.org:10.1105/tpc.17.00983
34 Boudolf, V. *et al.* The plant-specific cyclin-dependent kinase CDKB1;1 and transcription factor E2Fa-DPa control the balance of mitotically dividing and endoreduplicating cells in Arabidopsis. *Plant Cell* **16**, 2683-2692 (2004). https://doi.org:10.1105/tpc.104.024398
35 Wang, K. *et al.* The CDK inhibitor SIAMESE targets both CDKA;1 and CDKB1 complexes to establish endoreplication in trichomes. *Plant Physiol.* **184**, 165-175 (2020). https://doi.org:10.1104/pp.20.00271
36 Kumar, N. *et al.* Functional conservation in the SIAMESE-RELATED family of cyclin-dependent kinase inhibitors in land plants. *Plant Cell* **27**, 3065-3080 (2015). https://doi.org:10.1105/tpc.15.00489
37 Yang, K.-Z. *et al.* Phosphorylation of serine 186 of bHLH transcription factor SPEECHLESS promotes stomatal development in Arabidopsis. *Mol. Plant* **8**, 783-795 (2015). https://doi.org:10.1016/j.molp.2014.12.014
38 Claeys, H. & Inze, D. The agony of choice: how plants balance growth and survival under water-limiting conditions. *Plant Physiol* **162**, 1768-1779 (2013). https://doi.org:10.1104/pp.113.220921
39 Nowack, M. K. *et al.* Genetic framework of cyclin-dependent kinase function in *Arabidopsis*. *Dev. Cell* **22**, 1030-1040 (2012). https://doi.org:10.1016/j.devcel.2012.02.015

40 Vlieghe, K. *et al.* The DP-E2F-like gene *DEL1* controls the endocycle in *Arabidopsis thaliana*. *Curr Biol* **15**, 59-63 (2005). https://doi.org:10.1016/j.cub.2004.12.038
41 Fendrych, M. *et al.* Programmed cell death controlled by ANAC033/SOMBRERO determines root cap organ size in *Arabidopsis*. *Curr. Biol.* **24**, 931-940 (2014). https://doi.org:10.1016/j.cub.2014.03.025
42 Karimi, M., Inzé, D. & Depicker, A. GATEWAY^{TM} vectors for *Agrobacterium*-mediated plant transformation. *Trends Plant Sci.* **7**, 193-195 (2002). https://doi.org:10.1016/s1360-1385(02)02251-3
43 Decaestecker, W. *et al.* CRISPR-TSKO: a technique for efficient mutagenesis in specific cell types, tissues, or organs in Arabidopsis. *Plant Cell* **31**, 2868-2887 (2019). https://doi.org:10.1105/tpc.19.00454
44 Clough, S. J. & Bent, A. F. Floral dip: a simplified method for *Agrobacterium*-mediated transformation of *Arabidopsis thaliana*. *Plant J.* **16**, 735-743 (1998). https://doi.org:10.1046/j.1365-313x.1998.00343.x
45 De Veylder, L. *et al.* Functional analysis of cyclin-dependent kinase inhibitors of Arabidopsis. *Plant Cell* **13**, 1653-1667 (2001). https://doi.org:10.1105/tpc.010087

Acknowledgments

The authors thank Dr. Annick Bleys for critical reading and helping in preparing the manuscript and Mattias Vermeersch for the expertise on the drought phenotyping platform. This work was supported by grants of the Research Foundation Flanders (G011420N and G010820N). I.A. and M.D. acknowledge the support from a “Don Carlos Antonio Lopez” by El Programa Nacional de Becas from Paraguay predoc (BECAL #164/2017) and Research Foundation Flanders postdoc grant (12Q7923N), respectively.

Author contributions

L.D.V supervised the project. M.D., I.A, D.I., J.G. and L.D.V. designed the experiments. M.D., I.A., S.P., R.T.B., R.A.B. and I.V. performed experiments. M.D., I.A. and L.D.V. wrote and modified the manuscript. All authors read and approved the final manuscript.

Competing interests

The authors declare no competing interests.

Additional information

Supplementary information The online version contains supplementary material

FIGURES

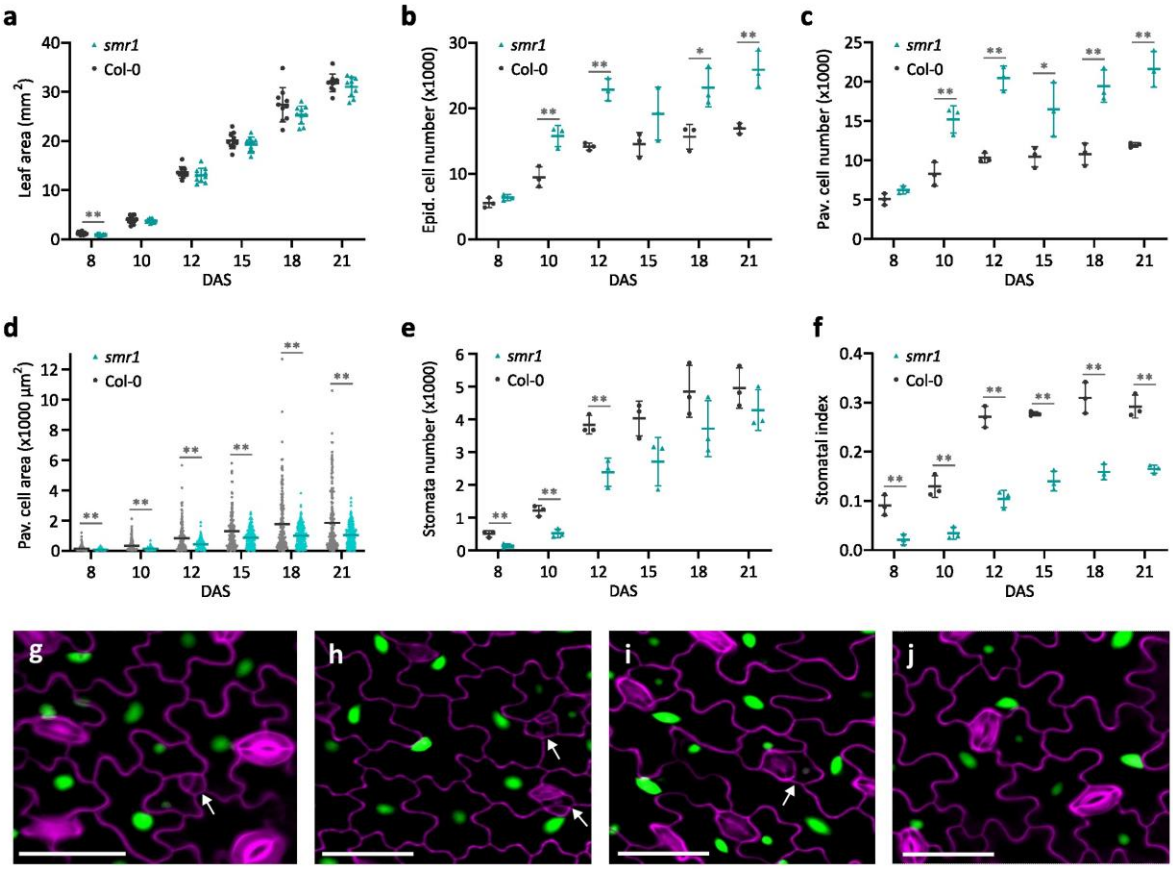

Fig. 1 SMR1 specifically controls epidermal pavement cell number. (a) Area of *smr1* mutant and wild-type first true leaves during development, from 8 to 21 days after stratification (DAS) (n > 10, mean +- SD, ** P<0.01, unpaired two-sided Student's t-test). **(b-f)** Total number of epidermal (b), pavement (c), and stomatal cells (d), pavement cell area (e), and stomatal index (f) in the abaxial epidermis of representative leaves described in (a) (n = 3, mean +- SD, with 60 - 200 cells analyzed per leaf, for (b,c,e,f-f) * = P<0.05 and ** P<0.01, unpaired two-sided Student's t-test and for (d) ** = P<0.001, Kolmogorov-Smirnov test). **(g-j)** Epidermal *pSMR1:GFP-GUS* localization. White arrows indicate SLGCs at different developmental stages, i.e. immediately after asymmetric division of the MMC into a meristemoid and SLGC (g) and when the SLGC is undergoing a spacing cell division (h) or developing lobes and sinuses (i). Eventually all cells surrounding the stoma express *SMR1* (j). Cell walls were visualized by propidum iodide (PI) staining (violet). Scale bars = 25 µm.

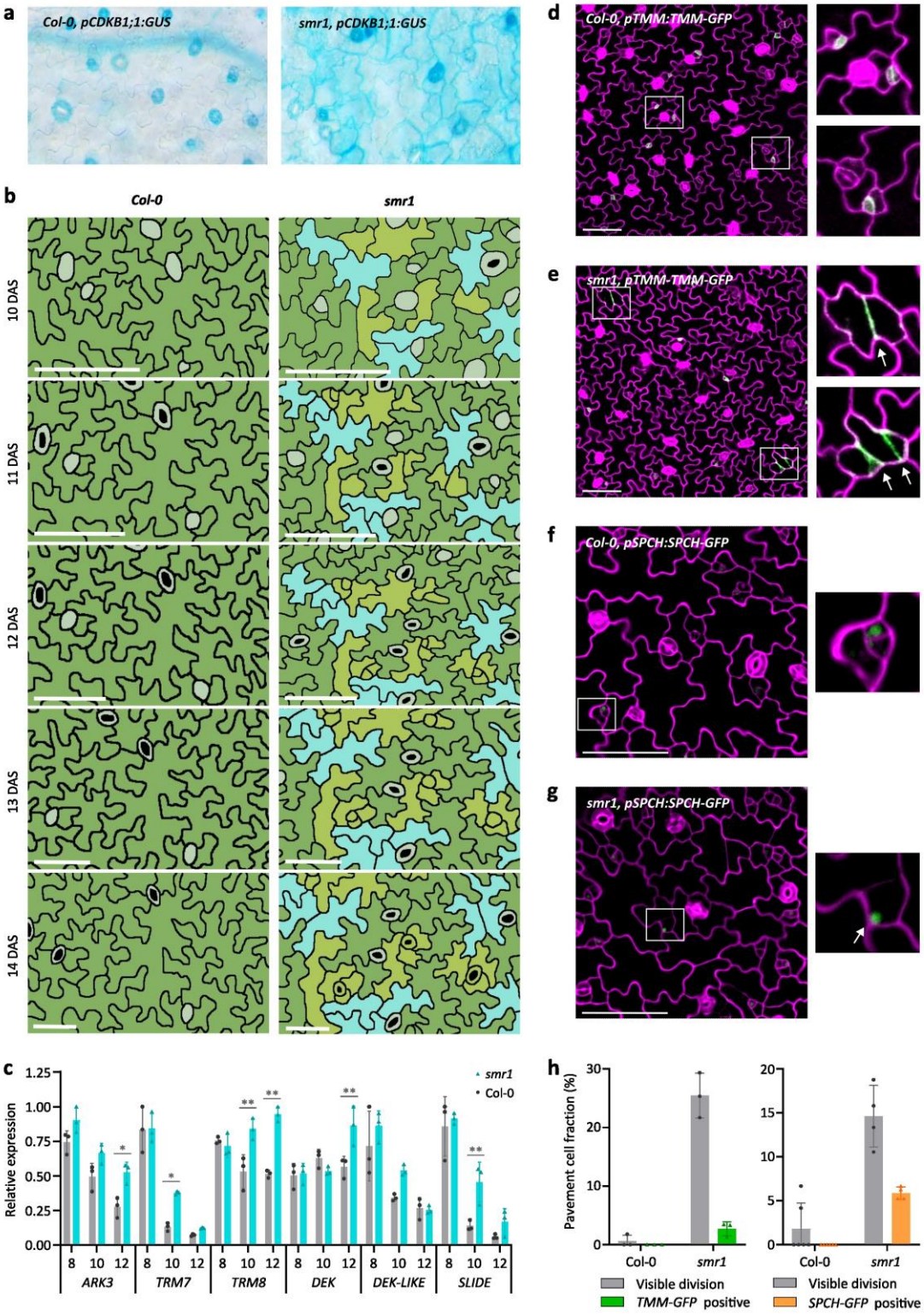

Fig. 2. ***smr1*** **mutant pavement cells behave like stomatal lineage ground cells. (a)** *pCDKB1;1:GUS* expression in wild-type versus *smr1* mutant 10-day-old first leaves. **(b)** Representative drawings of a time series (from 10 to 14 days after stratification, DAS) of Col-0

and *smr1* epidermis showing symmetrically (light blue colored cells) and asymmetrically (light green cells) dividing pavement cells. Guard mother cells and stomata are in gray. Scale bars = 25 μm. **(c)** RT-qPCR expression levels of SLGC division competency genes in 8- to 12-day-old wild-type (Col-0) and *smr1* mutant first leaves (n = 3, mean +- SD, * = P<0.05 and ** P<0.01, two-way ANOVA, Sidak's multiple comparison tests). **(d-g)** *TMM-GFP* (d,e) and *SPCH-GFP* (f,g) expression in cotyledons of Col-0 (d,f) and *smr1* (e,g). Cells walls were visualized by PI staining (violet). White boxes indicate the region of the inset (right panels), white arrows in insets indicate the GFP signal in newly dividing pavement cells. Scale bars = 50 μm. **(h)** Quantification of dividing pavement cells and *TMM-GFP* and *SPCH-GFP* expressing cells in Col-0 and *smr1* epidermis (n = 3 biologically independent samples (leaves) for TMM quantification (left), n = 5 biologically independent samples (leaves) for SPCH quantification (right) in smr1 and n = 6 biologically independent samples (leaves) for SPCH quantification in the wild type, with 70 – 200 pavement cells analyzed per line, mean +- SD).

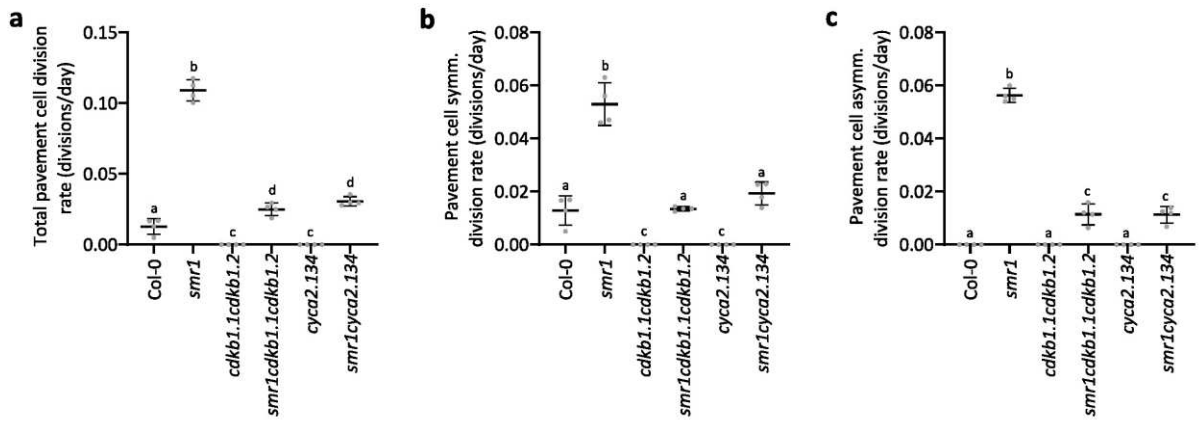

Fig. 3. Pavement cell division rates of *smr1*, *cdkb1;1 ckdb1;2, smr1 cdkb1;1 cdkb1;2, cyca2;1 cyca2;3 cyca2;4 (cyca2.134) and smr1 cyca2.134* mutant leaves. (a-c) Pavement cell division rates were determined by dental prints. Rates of overall pavement cell division (a), symmetric division (b) and asymmetric division giving rise to stomata (c). Letters indicate statistically different means (mean +- SD, $P < 0.05$, one-way ANOVA, Tukey's multiple comparison tests, $n \geq 4$ leaves, number of cells ≥ 180).

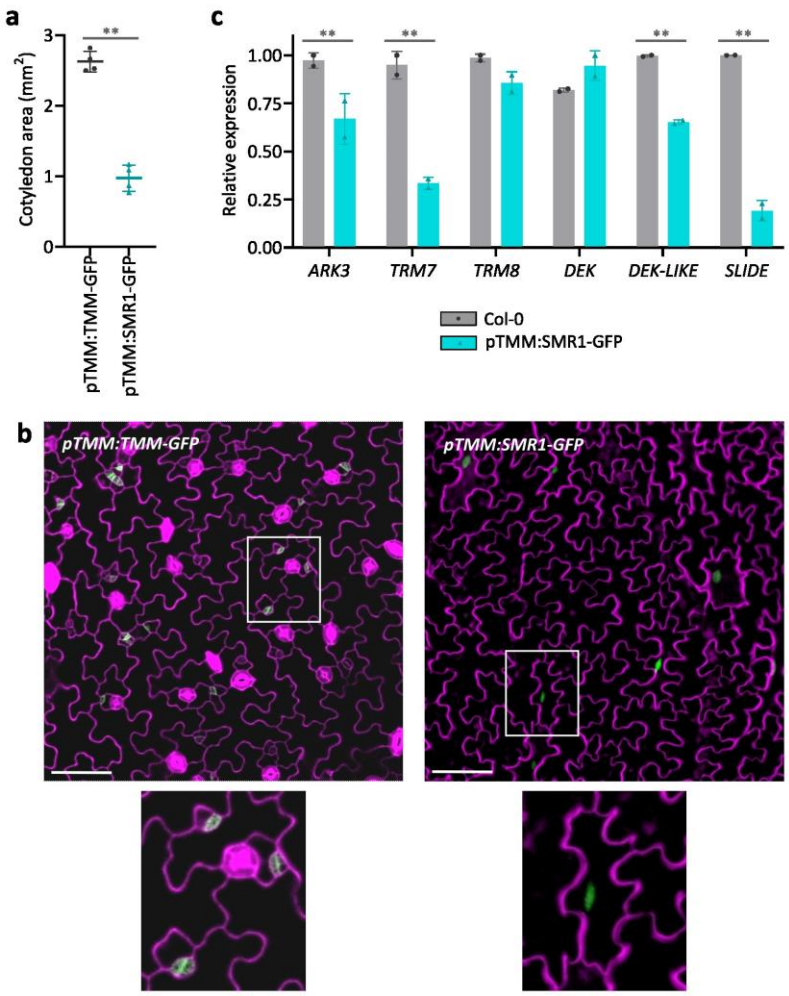

Fig. 4. Ectopic *SMR1* expression triggers pavement cell differentiation of stomatal precursor cells. (a) Cotyledon area of 5-day-old *pTMM:TMM-GFP* and *pTMM:SMR1-GFP* cotyledons (n = 4, mean +- SD, ** P<0.001, unpaired two-sided Student's t-test). **(b)** *pTMM:TMM-GFP* (left panels) and *pTMM:SMR1-GFP* (right panels) expression in the abaxial epidermis of cotyledons at 5 DAS. Cell walls were visualized by PI staining (violet). White boxes indicate the region of the insets at the bottom, showing GFP-positive cells. Note that b shows the same zone as in Figure 2d. Scale bars = 50 µm. **(c)** RT-qPCR expression levels of SLGC division competency genes in *Col-0* versus *pTMM:SMR1-GFP* cotyledons at 5 DAS (n = 2, mean +- SD, ** = P< 0.001, two-way ANOVA, Sidak's multiple comparison tests).

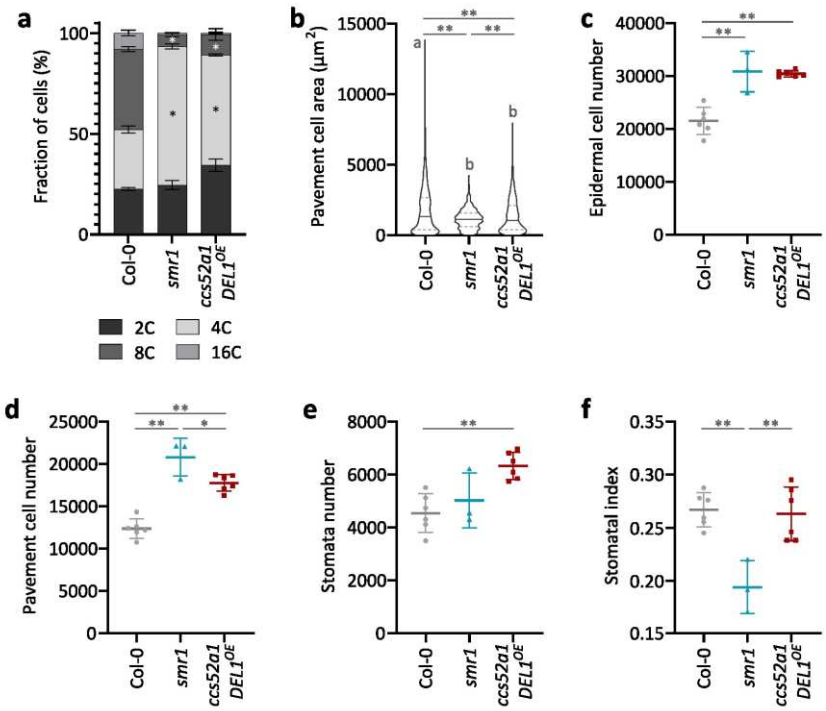

Fig. 5. The *smr1* mutant epidermal phenotype is not solely caused by reduced ploidy levels. **(a)** Epidermis-specific ploidy distribution in the *smr1* mutant and the *ccs52a1 DEL1^{OE}* double mutant in which two other endoreplication pathways are affected (* = P<0.05, two-way ANOVA, Tukey's multiple comparison tests, n = 3, with ≥ 4000 epidermal cells per sample, mean +- SD). **(b)** Distribution of pavement cell area in Col-0, *smr1* and the *ccs52a1 DEL1^{OE}* double mutant of 21-day-old first leaves. The plain line indicates the median, the dashed lines the 25% and 75% percentiles. Letters indicate statistically different means (P< 0.001, ANOVA with Kruskal-Wallis multiple comparison test) and asterisks indicate statistically significant changes in the distribution (** = P< 0.001, Kolmogorov-Smirnov test, n ≥ 3 leaves, number of cells per leaf ≥ 60). **(c-f)** Total number of epidermal cells (c), pavement cells (d), stomata (e) and the stomatal index (f) of Col-0, *smr1* and the *ccs52a1 DEL1^{OE}* double mutant of 21-day-old first leaves (* = P< 0.05 and ** = P< 0.001, one-way ANOVA, Tukey's multiple comparison tests, n ≥ 3 leaves, number of cells per leaf ≥ 60, mean +- SD,).

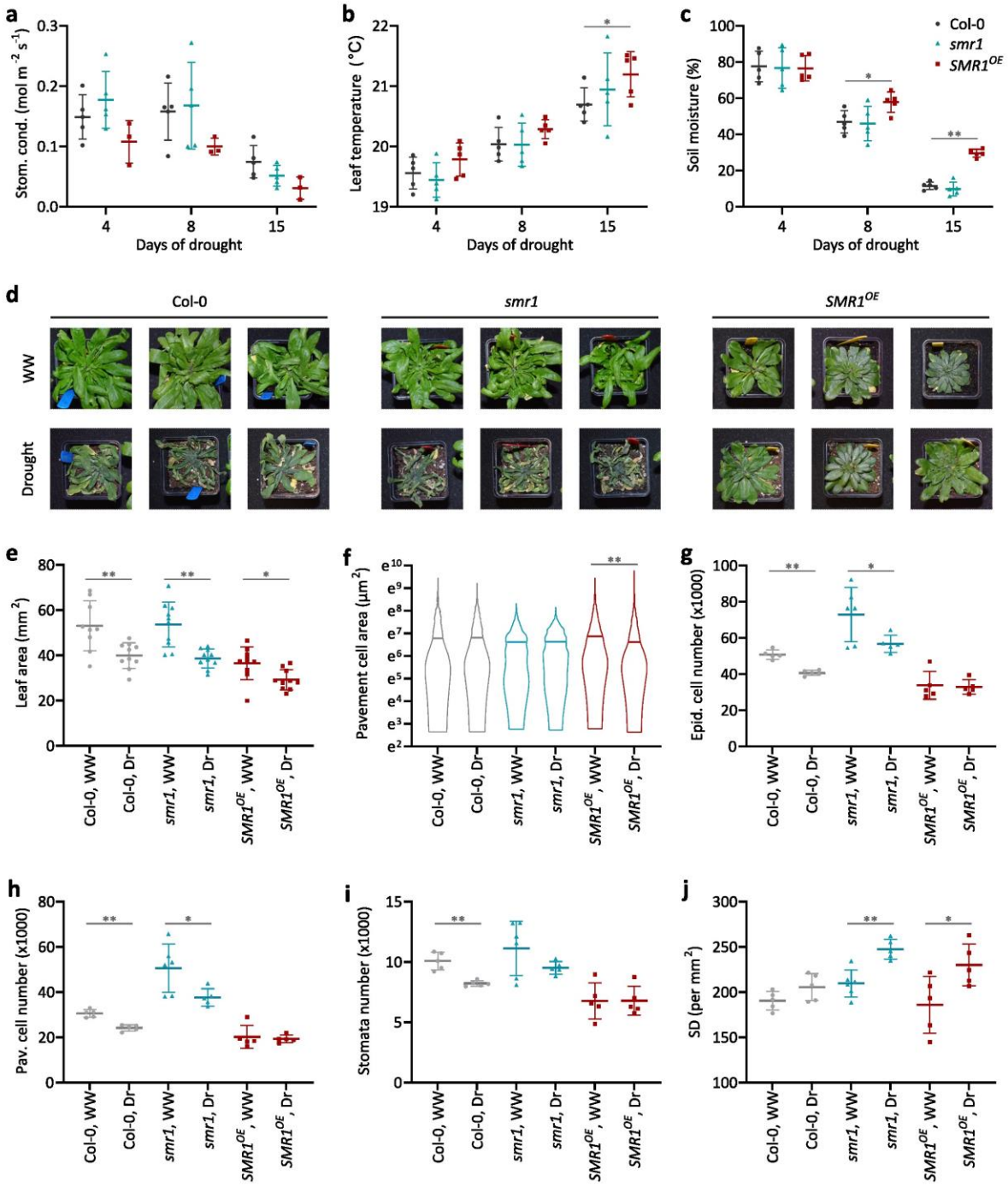

Fig. 6. SMR1 controls stomatal density under drought conditions. (a-c) Time series of stomatal conductance (a), leaf temperature (b) and soil moisture (c) measured during dehydration of 5-week-old rosettes of wild-type, *smr1* and *SMR1*^{OE} plants (* = P< 0.05 and ** = P< 0.001, two-way ANOVA, Dunnett's multiple comparison tests, n ≥ 3, mean +- SD). **(d)** Representative images of 7-week-old rosettes of wild-type, *smr1* and *SMR1*^{OE} plants. Drought-stressed plants underwent 2 weeks of dehydration, well-watered (WW) plants were watered daily. **(e)** Leaf area of the third leaf of 19-day-old plants of the lines mentioned above, exposed to moderate drought (Dr) stress or WW conditions (n = 10, * = P<0.05 and ** P<0.01, unpaired two-sided Student's t-test, mean +-

SD). **(f)** Distribution of pavement cell area of the leaves mentioned in (e). Asterisks indicate statistically significant changes in the distribution (** = P< 0.001, Kolmogorov-Smirnov test, n ≥ 5 leaves, number of cells per leaf ≥ 140). **(g-j)** Total number of epidermal cells (g), pavement cells (h), stomata (i) and the stomatal density (j, SD) of the leaves mentioned in (e) (n ≥ 5 leaves, * = P<0.05 and ** P<0.01, unpaired two-sided Student's t-test, mean +- SD).